Journal of Fluorescence (2018) 28:913–931
https://doi.org/10.1007/s10895-018-2254-z

ORIGINAL ARTICLE

# Comparative DFT Computational Studies with Experimental Investigations for Novel Synthesized Fluorescent Pyrazoline Derivatives

Ahmad Saed Salim[1] · Adel S. Girgis[2] · Altaf H. Basta[3] · Houssni El-saied[3] · Mohamed A. Mohamed[1] · Ahmad H. Bedair[4]

Received: 2 May 2018 / Accepted: 7 June 2018 / Published online: 29 June 2018


**Abstract**
A novel series of pyrazoline derivatives were synthesized and their spectral properties were characterized via FT-IR, $^{1}H$, and $^{13}C$ NMR. The electronic transitions and fluorescence properties were tracked via UV-Vis and emission spectrometry. The density functional theory (DFT) calculations have been also computed to get spot onto the geometry, electronic transitions and spectroscopic properties theoretically that has been compared with the encountered experimental ones. Moreover, the dipole moment, optimized energy, HOMO - LUMO energies and band gaps were calculated for novel candidates pyrazoline derivatives with highly fluorescence quantum yield.

**Keywords** DFT computations · 2-pyrazoline · FMOs · MEP · NMR · FT-IR

## Introduction

Pyrazolines are one of the most important five-membered heterocycles that have received lots of attention in organic synthesis [1–4]. Due to the presence of dihydro pyrazoles in their chemical structures as a central core in all derivatives they possess a wide spectrum of biological activities such as anticancer, anti-inflammatory, antiviral and antibacterial activities [5–9]. Especially, 1,3,5-Triaryle-2-pyrazolines, are used widely in fluorescent dyes due to their emitting vivid blue fluorescence with prominent and high fluorescence quantum yield [10–16]. Moreover, intermolecular charge transfer (ICT) is attracting phenomenon that is typically achieved for pyrazoline derivatives [17]. With great progress industrially pyrazolines are used as brightening agents in textile manufacture, paper and plastic fabrication [18–23].

In the present work, we reported the synthesis of twenty-one novel 1,3,5-triaryl-2-pyrazolines as mention in details on our previous work [24]. Then we select four synthesized active novel pyrazolines and named with 13, 15, 18 and 23 due to their prominent fluorescence quantum yield (0.819, 0.858, 0.553, 0.844) than quinine sulfate (reference).

The density functional theory (DFT) calculations are applied for the selected (13,15,18 and 23) compounds. All the experimental investigations observed data were compared with theoretical computations obtained from DFT calculations.

## Experimental

### Instrumentation

The FT-IR spectra (KBr) were recorded on a shimadzu FT-IR 8400S spectrophotometer. UV-vis spectra were recorded on a shimadzu UV-1800 spectrophotometer. Emission spectra were measured on a LUMINA fluorescence spectrometer. 1H-NMR spectra were measured on a Varian Mercury 300 (300 MHz) and a Bruker Ascend 400/R (400 MHz) spectrometer. $^{13}C$-NMR spectra were recorded on a Bruker Ascend

**Electronic Supplementary Material** The online version of this article (https://doi.org/10.1007/s10895-018-2254-z) contains supplementary material, which is available to authorized users.

✉ Ahmad Saed Salim
ascholar_ahmad2006@yahoo.com; Ahmedsaed.fm@jp.gov.eg

[1] Forgery Research Department, Forensic Medicine Authority, Ministry of Justice, Cairo 11381, Egypt

[2] Pesticide Chemistry Department, National Research Center, Dokki, Giza 12622, Egypt

[3] Cellulose and Paper Department, National Research Center, Dokki, Giza 12622, Egypt

[4] Chemistry Department, Faculty of Science, Al-Azhar University, Cairo, Egypt

400/R (100 MHz) spectrometer. Melting points were recorded on a Stuart SMP3 melting point apparatus.

## Synthesis General Procedure

A mixture of equimolar amounts of the appropriate 1,3-diaryl-2-propen-1-ones **1–9** (5 mmol) and the corresponding aryl hydrazines **10–12** (the hydrochloride salt was used in case of **11** and **12**) in absolute ethanol (15 ml) was boiled under reflux (TLC control). The solid separated upon storing the reaction mixture at room temperature overnight, was collected and crystallized from a suitable solvent affording the corresponding pyrazolines **13–33** (Scheme 1).

## Experimental Characterization of the Selected Pyrazolines 13, 15, 18 and 23

The chemical structures of selected compounds 13, 15, 18 and 23 are given in Scheme 2. The details of synthesis procedures for selected four compounds are reported as viz.:

**3-(4-Chlorophenyl)-5-(4-fluorophenyl)-1-phenyl-4,5-dihydro-1*H*-pyrazole (13)**

Obtained from reaction of **1** and **10**. Reaction time 6 h, almost colorless microcrystals from n-butanol, mp 156–158 °C, yield 89% (1.55 g). IR $\nu$ ($cm^{-1}$): 1589, 1558, 1504, 1493. $^1$H-NMR δ (ppm): (300 MHz) 3.08 (dd, $J$ = 7.5, 17.1 Hz, 1H, upfield H of pyrazolinyl $H_2C$-4), 3.81 (dd, $J$ = 12.5, 17.0 Hz, 1H, downfield H of pyrazolinyl $H_2C$-4), 5.28 (dd, $J$ = 7.2, 12.3 Hz, 1H, pyrazolinyl *HC*-5), 6.78–6.85 (m, 1H, arom. H), 7.01–7.43 (m, 10H, arom. H), 7.65 (d, $J$ = 8.7 Hz, 2H, arom. H). $^{13}$C-NMR δ (ppm): (100 MHz) 43.4 (pyrazolinyl $H_2C$-4), 64.0 (pyrazolinyl H*C*-5), 113.5, 116.0, 116.2, 119.5, 125.3, 126.9, 127.1, 127.5, 127.6, 128.8, 128.9, 129.0, 129.1, 131.2, 134.4, 138.0, 138.1, 144.5, 145.6, 161.0, 163.4 (arom. *C*). Elemental analysis: $C_{21}H_{16}ClFN_2$ required C, 71.90; H, 4.60; N, 7.99, found C, 72.09; H, 4.71; N, 8.07.

**5-(4-Fluorophenyl)- 3-(4-methylphenyl)-1-phenyl-4,5-dihydro-1H-pyrazole (15)**

Obtained from reaction of **3** and **10**. Reaction time 9 h, pale yellow microcrystals from n-butanol, mp 147–149 °C, yield 82% (1.35 g). IR $\nu$ ($cm^{-1}$): 1597, 1551, 1497. $^1$H-NMR δ (ppm): (300 MHz) 2.39 (s, 3H, *CH*$_3$), 3.10 (dd, $J$ = 7.4, 17.0 Hz, 1H, upfield H of pyrazolinyl $H_2C$-4), 3.83 (dd, $J$ = 12.5, 17.0 Hz, 1H, downfield H of pyrazolinyl $H_2C$-4), 5.24 (dd, $J$ = 7.2, 12.3 Hz, 1H, pyrazolinyl *HC*-5), 6.79–7.64 (m, 13H, arom. H). $^{13}$C-NMR δ (ppm): (100 MHz) 21.4 (*C*H$_3$), 43.7 (pyrazolinyl $H_2C$-4), 63.8 (pyrazolinyl H*C*-5), 113.4, 115.9, 116.1, 119.2, 125.8, 127.5, 127.6, 129.0, 129.3, 129.9, 138.4, 138.5, 138.8, 144.9, 145.0, 160.9, 163.4 (arom. *C*).

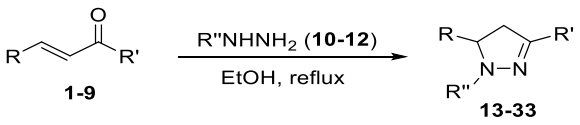


**1**; R = 4-$FC_6H_4$, R' = 4-$ClC_6H_4$
**2**; R = 4-$FC_6H_4$, R' = 4-$BrC_6H_4$
**3**; R = 4-$FC_6H_4$, R' = 4-$H_3CC_6H_4$
**4**; R = 4-$FC_6H_4$, R' = 4-$H_3COC_6H_4$
**5**; R = 4-$FC_6H_4$, R' = 2-Thienyl
**6**; R = 4-$FC_6H_4$, R' = 2-Naphthyl
**7**; R = 2-Naphthyl, R' = 4-$FC_6H_4$
**8**; R = 2,4-$Cl_2C_6H_3$, R' = 4-$FC_6H_4$
**9**; R = 2,5-$(H_3CO)_2C_6H_3$, R' = 4-$FC_6H_4$

**10**, R" = Ph
**11**, R" = 4-$ClC_6H_4$
**12**, R" = 4-$H_3CC_6H_4$

**13**; R = 4-$FC_6H_4$, R' = 4-$ClC_6H_4$, R" = Ph
**14**; R = 4-$FC_6H_4$, R' = 4-$BrC_6H_4$, R" = Ph
**15**; R = 4-$FC_6H_4$, R' = 4-$H_3CC_6H_4$, R" = Ph
**16**; R = 4-$FC_6H_4$, R' = 4-$H_3COC_6H_4$, R" = Ph
**17**; R = 4-$FC_6H_4$, R' = 2-Thienyl, R" = Ph
**18**; R = 4-$FC_6H_4$, R' = 2-Naphthyl, R" = 4-$ClC_6H_4$
**19**; R = 4-$FC_6H_4$, R' = R" = 4-$ClC_6H_4$
**20**; R = 4-$FC_6H_4$, R' = 4-$BrC_6H_4$, R" = 4-$ClC_6H_4$
**21**; R = 4-$FC_6H_4$, R' = 4-$H_3COC_6H_4$, R" = 4-$ClC_6H_4$
**22**; R = 4-$FC_6H_4$, R' = 2-Thienyl, R" = 4-$ClC_6H_4$
**23**; R = 4-$FC_6H_4$, R' = 2-Naphthyl, R" = 4-$H_3CC_6H_4$
**24**; R = 4-$FC_6H_4$, R' = 4-$BrC_6H_4$, R" = 4-$H_3CC_6H_4$
**25**; R = 4-$FC_6H_4$, R' = 4-$H_3COC_6H_4$, R" = 4-$H_3CC_6H_4$
**26**; R = 4-$FC_6H_4$, R' = 2-Thienyl, R" = 4-$H_3CC_6H_4$
**27**; R = 2-Naphthyl, R' = 4-$FC_6H_4$, R" = 4-$ClC_6H_4$
**28**; R = 2-Naphthyl, R' = 4-$FC_6H_4$, R" = 4-$H_3CC_6H_4$
**29**; R = 2,4-$Cl_2C_6H_3$, R' = 4-$FC_6H_4$, R" = 4-$ClC_6H_4$
**30**; R = 2,4-$Cl_2C_6H_3$, R' = 4-$FC_6H_4$, R" = 4-$H_3CC_6H_4$
**31**; R = 2,5-$(H_3CO)_2C_6H_3$, R' = 4-$FC_6H_4$, R" = Ph
**32**; R = 2,5-$(H_3CO)_2C_6H_3$, R' = 4-$FC_6H_4$, R" = 4-$ClC_6H_4$
**33**; R = 2,5-$(H_3CO)_2C_6H_3$, R' = 4-$FC_6H_4$, R" = 4-$H_3CC_6H_4$

**Scheme 1** The selected synthetic approach for 2-prazolines 13–33

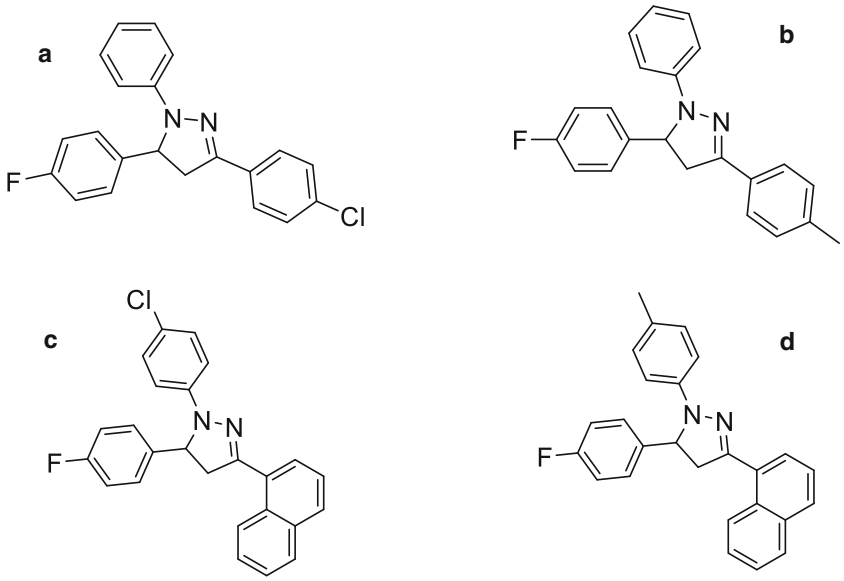


**Scheme 2** The chemical structures of (**a**) compound 13, (**b**) compound 15, (**c**) compound 18 and (**d**) compound 23

Elemental analysis: $C_{22}H_{19}FN_2$ required C, 79.97; H, 5.80; N, 8.48, found C, 80.04; H, 5.92; N, 8.64.

**1-(4-Chlorophenyl)-5-(4-fluorophenyl)-3-(2-naphthyl)-4,5-dihydro-1H-pyrazole (18)**

Obtained from reaction of **6** and **11**. Reaction time 8 h, pale yellow microcrystals from n-butanol, mp 184–186 °C, yield 80% (1.60 g). IR $\nu$ ($cm^{-1}$): 1595, 1495, 1439. $^1$H-NMR $\delta$ (ppm): (400 MHz) 3.25 (dd, $J$ = 7.0, 17.0 Hz, 1H, upfield H of pyrazolinyl $H_2C$-4), 3.93 (dd, $J$ = 12.3, 17.0 Hz, 1H, downfield H of pyrazolinyl $H_2C$-4), 5.26 (dd, $J$ = 7.0, 12.2 Hz, 1H, pyrazolinyl *HC*-5), 7.03–7.08 (m, 4H, arom. H), 7.16–7.19 (m, 2H, arom. H), 7.28–7.32 (m, 2H, arom. H), 7.50–7.53 (m, 2H, arom. H), 7.81–7.88 (m, 4H, arom. H), 8.17 (dd, J = 1.6, 8.6 Hz, 1H, arom. H). $^{13}$C-NMR $\delta$ (ppm): (100 MHz) 43.6 (pyrazolinyl $H_2C$-4), 63.9 (pyrazolinyl H*C*-5), 114.6, 116.1, 116.3, 123.4, 124.2, 125.4, 126.4, 126.58, 126.59, 127.5, 127.6, 127.9, 128.1, 128.3, 128.9, 129.2, 130.0, 133.3, 133.6, 137.7, 137.8, 143.1, 147.4, 161.0, 163.5 (arom. *C*). Elemental analysis: $C_{25}H_{18}ClFN_2$ required C, 74.90; H, 4.53; N, 6.99, found C, 75.12; H, 4.71; N, 7.18.

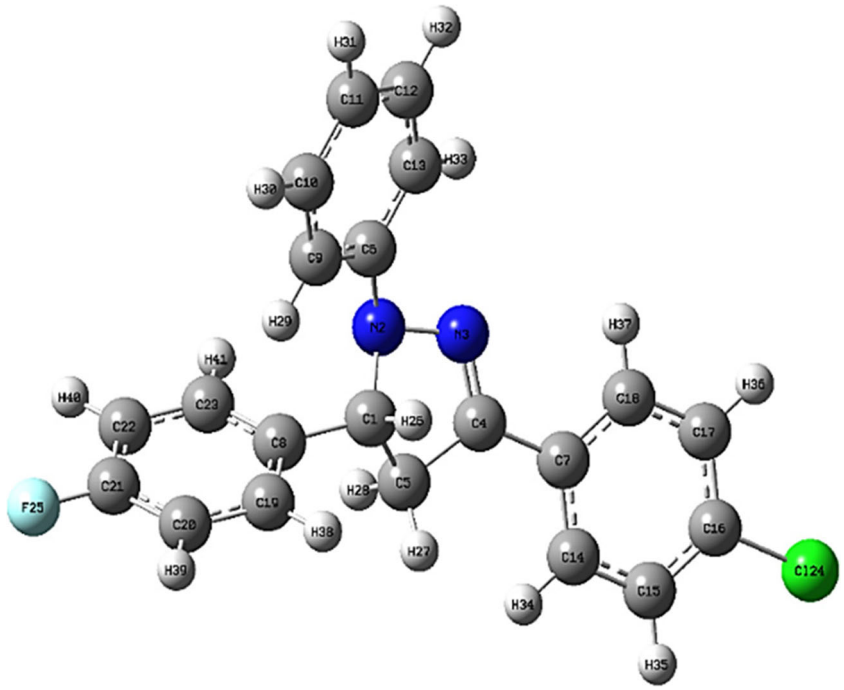


**Fig. 1** The optimized molecular geometry of compound 13 at DFT (B3LYP) with 6–31 G(d, p) basis set in gas phase

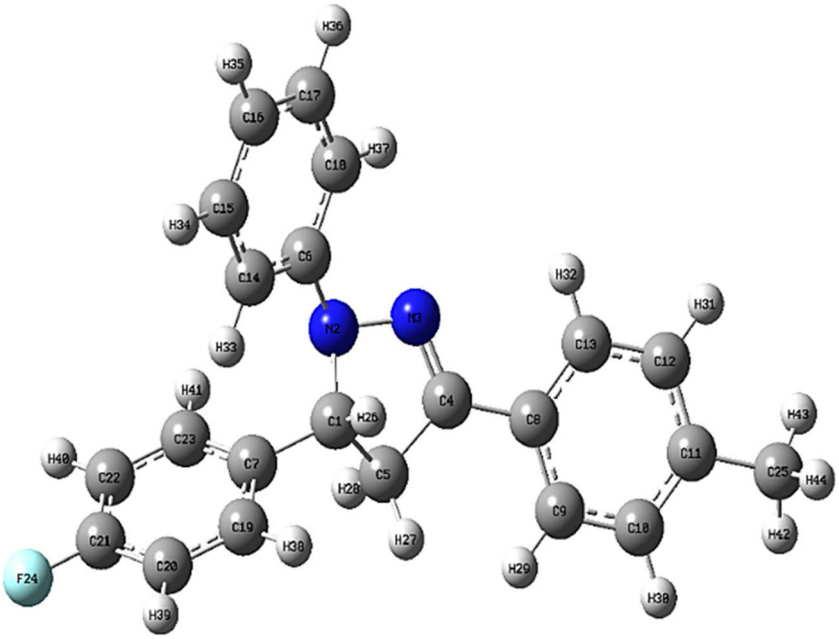


**Fig. 2** The optimized molecular geometry of compound 15 at DFT (B3LYP) with 6–31 G(d, p) basis set in gas phase

**5-(4-Fluorophenyl)-1-(4-methylphenyl)-3-(2-naphthyl)-4,5-dihydro-1H-pyrazole (23)**

Obtained from reaction of **6** and **12**. Reaction time 6 h, pale yellow microcrystals from n-butanol, mp 188–189 °C, yield 84% (1.60 g). IR $\nu$ ($cm^{-1}$): 1602, 1558, 1516, 1504. $^{1}$H-NMR δ (ppm): (400 MHz) 2.28 (s, 3H, $CH_3$), 3.25 (dd, $J$ = 7.4, 16.9 Hz, 1H, upfield H of pyrazolinyl $H_2C$-4), 3.91–3.99 (m, 1H, downfield H of pyrazolinyl $H_2C$-4), 5.27–5.32 (m, 1H, pyrazolinyl $HC$-5), 7.04–7.08 (m, 6H, arom. H), 7.28–7.36 (m, 2H, arom. H), 7.48–7.51 (m, 2H, arom. H), 7.81–7.88 (m, 4H, arom. H), 8.19 (d, $J$ = 8.7 Hz, 1H, arom. H). $^{13}$C-NMR $\delta$ (ppm): (100 MHz) 20.5 ($CH_3$), 43.5 (pyrazolinyl $H_2C$-4), 64.2 (pyrazolinyl

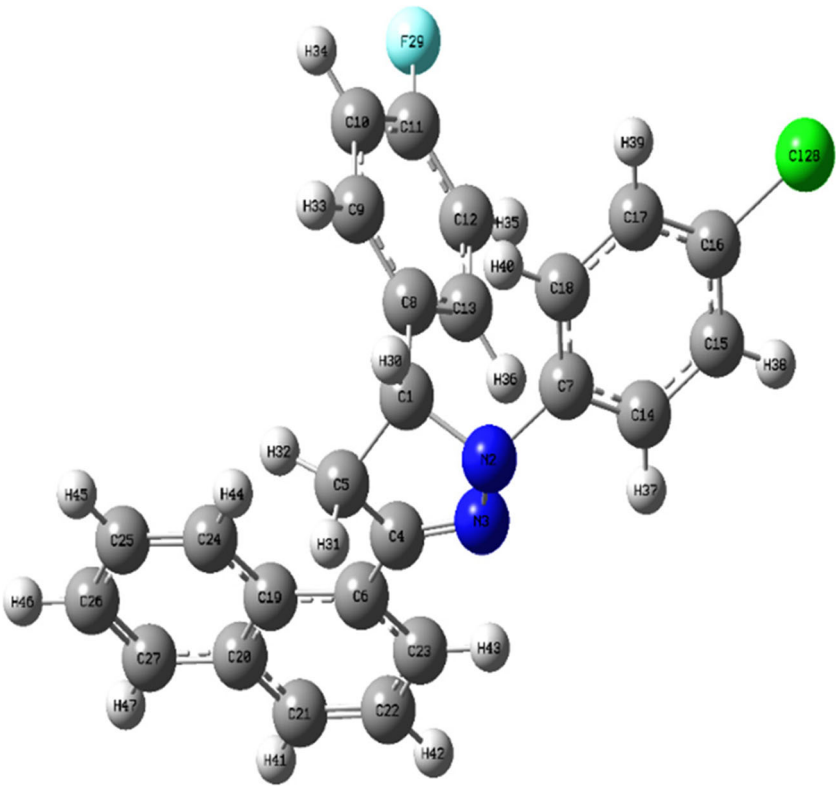


**Fig. 3** The optimized molecular geometry of compound 18 at DFT (B3LYP) with 6–31 G(d, p) basis set in gas phase

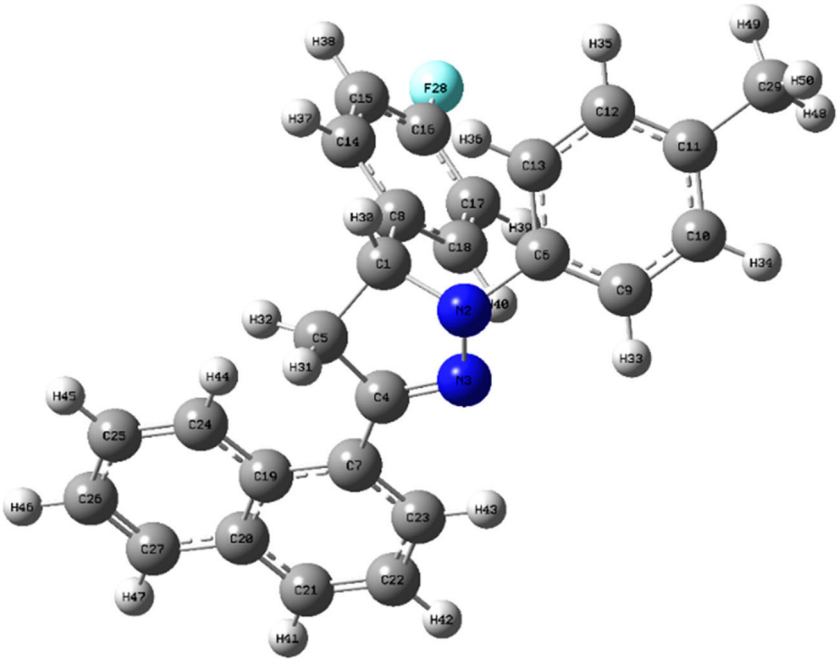


**Fig. 4** The optimized molecular geometry of compound 23 at DFT (B3LYP) with 6–31 G(d, p) basis set in gas phase

H*C*-5), 113.6, 115.9, 116.1, 123.5, 125.0, 125.4, 126.3, 126.5, 127.6, 127.7, 127.8, 128.1, 128.2, 128.7, 129.5, 129.7, 130.4, 133.3, 133.4, 138.39, 138.42, 142.5, 146.4, 160.9, 163.4 (arom. *C*). Elemental analysis: $C_{26}H_{21}FN_2$ required C, 82.08; H, 5.56; N, 7.36, found C, 82.24; H, 5.67; N, 7.22.

## Computational Details

All computations were performed with the Gaussian 09 W program package [25] with Gaussian View 6 molecular visualization program [26]. The hybrid Becke-3 function with Lee-Yang-Parr correlation function (B3LYP) method [27] of density functional theory (DFT) with 6-31G (d,p) basis set [28] in the gas phase was applied for prediction of molecular geometries and calculations of vibrational frequencies. For the molecular geometry optimization, no symmetry constraints were applied. The computed vibrational frequency values were scaled with a scaling factor 0.9613 and no imaginary frequencies were obtained from calculations. Time- dependent functional theory (TD-DFT) was performed to simulate the UV-vis spectra at B3LYP/6-31G (d,p) level of theory in the gas phase for the optimized structured at the ground state. The excited states at the same level of theory of TD-DFT were optimized to obtain the simulated emission spectra. $^{1}H$ and $^{13}C$ NMR computations were performed using the gauge-invariant atomic orbital (GIAO) method at B3LYP/6–311 + G(2d,p) in gas phase after the

**Table 1** The selected bond distances, bond angles and dihedral angles for compound 13

| Connectivity | Bond distance (Å) | Connectivity | Bond angle ( ) | Connectivity | Dihedral angle ( ) |
|---|---|---|---|---|---|
| C1-N2 | 1.481 (1.470) | C1-N2-N3 | 112.98 (111.90) | C6-N2-C1-C5 | −163.44 (161.13) |
| N2-N3 | 1.364 (1.426) | C1-N2-C6 | 125.07 (108.00) | C7-C4-N3-N2 | 178.33 (178.89) |
| N3-C4 | 1.294 (1.260) | C7-C1-N2 | 122.20 (120.00) | C8-C1-N2-N3 | −121.29 (−137.89) |
| C4-C5 | 1.517 (1.497) | C8-C4-N3 | 113.42 (110.91) | C9-C6-N2-N3 | −10.31 (18) |
| N2-C6 | 1.390 (1.462) | C9-C8-C4 | 120.47 (120.00) | C14-C7-C4-N3 | 178.85 (114.83) |
| C1-C8 | 1.521 (1.497) | C14-C6-N2 | 120.72 (120.00) | C19-C8-C1-N2 | −146.90 (−122.76) |
| C4-C7 | 1.461 (1.503) | C19-C7-C1 | 119.97 (121.40) | | |
| C16-Cl24 | 1.758 (1.719) | | | | |
| C21-F25 | 1.349 (1.320) | | | | |

*The values in the parenthesis are taken from reference [29]

**Table 2** The selected bond distances, bond angles and dihedral angles for compound 15

| Connectivity | Bond distance (Å) | Connectivity | Bond angle ( ) | Connectivity | Dihedral angle ( ) |
|---|---|---|---|---|---|
| C1-N2 | 1.480 (1.470) | C1-N2-N3 | 112.88 (111.90) | C6-N2-C1-C5 | −162.37 (161.13) |
| N2-N3 | 1.369 (1.426) | C6-N2-C1 | 124.76 (108.00) | C7-C1-N2-N3 | −122.98 (−137.88) |
| N3-C4 | 1.293 (1.260) | C7-C1-N2 | 113.47 (110.90) | C8-C4-N3-N2 | 178.18 (178.89) |
| C4-C5 | 1.517 (1.497) | C8-C4-N3 | 122.41 (120.00) | C14-C6-N2-N3 | −11.95 (−162.00) |
| N2-C6 | 1.399 (1.462) | C9-C8-C4 | 120.85 (120.00) | C9-C8-C4-N3 | 179.08 (114.83) |
| C1-C7 | 1.521 (1.497) | C14-C6-N2 | 120.54 (120.00) | C19-C7-C1-N2 | −147.27 (−122.76) |
| C4-C8 | 1.462 (1.503) | C19-C7-C1 | 120.00 (121.40) | C14-C6-N2-C1 | −11.95 (18) |
| C11-C25 | 1.509 (1.497) | | | | |
| C21-F24 | 1.350 (1.320) | | | | |

*The values in the parenthesis are taken from reference [30]

molecular geometry was optimized at the same level of theory. Furthermore, the dipole moment, energy of optimization, HOMO-LUMO analysis and molecular electrostatic potential (MEP) maps for selected compounds were calculated via DFT/B3LYP method using 6–31 G (d,p) basis set in the gas phase and their 3D plots were visualized at the same level of theory.

## Optimized Molecular Geometries

For compounds 13, 15, 18 and 23, the optimized molecular structures are computed via DFT using B3LYP method and 6-31G (d,p) basis set, with the numbering of atoms, are presented in Figs. 1, 2, 3, and 4. The complete optimized molecular geometry parameters for candidate compounds are given in Tables (1S–4S). The selected optimized molecular geometry parameters for given compounds in the gas phase are presented in Tables 1, 2, 3, and 4.

As seen from the selected tables of optimized geometry parameters for compounds 13, 15, 18 and 23, the N-N bond lengths located in the core ring (pyrazoline ring), are 1.364, 1.369, 1.371 and 1.369 respectively, in excellent consistent with optimal compared experimental references data. At the same circumstance, the computed bond lengths ascribed to N2-C6, N2-C6, N2-C7 and N2-C6 for compounds 13, 15, 18 and 23 respectively, were found as 1.390, 1.399, 1.393 and 1.397 correspondingly, in good agreement with corresponding experimental references data. Additionally, the selected bond angles connectivity presented in Tables 1, 2, 3, and 4 exhibited minor slightly deviations than the optimal bond angles recorded experimentally. Furthermore, the aromatic rings planarity connected to the core ring (pyrazoline ring) can be illustrated via computed dihedral angles values. From the calculated dihedral angles presented in tables (1S–4S), we found that the pyrazoline ring for compounds 13, 15, 18 and 23 respectively, didn't planar. Also, an aromatic ring connected to the N2 nitrogen atom in the core ring is co-planar. In a contrary, both aromatic rings that are connected to

**Table 3** The selected bond distances, bond angles and dihedral angles for compound 18

| Connectivity | Bond distance (Å) | Connectivity | Bond angle ( ) | Connectivity | Dihedral angle ( ) |
|---|---|---|---|---|---|
| C1-N2 | 1.476 (1.470) | C1-N2-N3 | 112.66 (111.90) | C7-N2-C1-C5 | −172.00 (161.13) |
| N2-N3 | 1.371 (1.426) | C1-N2-C7 | 126.33 (108.00) | C6-C4-N3-N2 | −174.48 (178.89) |
| N3-C4 | 1.293 (1.260) | C6-C4-N3 | 121.27 (120.00) | C8-C1-N3-N2 | −104.90 (−137.88) |
| C4-C5 | 1.523 (1.497) | C8-C1-N2 | 113.51 (110.91) | C14-C7-N2-N3 | −176.07 (−168.94) |
| N2-C7 | 1.393 (1.462) | C9-C8-C1 | 119.77 (120.00) | C9-C8-C1-N2 | −149.66 (−122.76) |
| C1-C8 | 1.524 (1.497) | C14-C7-N2 | 120.58 (120.00) | C19-C6-C4-N3 | −135.21 (−107.61) |
| C4-C6 | 1.476 (1.503) | C19-C6-C4 | 122.27 (120.00) | C18-C7-N2-C1 | (11.06) |
| C20-C19 | 1.435 (1.497) | | | | |
| C16-Cl26 | 1.762 (1.719) | | | | |
| C11-F29 | 1.349 (1.320) | | | | |

*The values in the parenthesis are taken from reference [31]

**Table 4** The selected bond distances, bond angles and dihedral angles for compound 23

| Connectivity | Bond distance (Å) | Connectivity | Bond angle ( ) | Connectivity | Dihedral angle ( ) |
|---|---|---|---|---|---|
| C1-N2 | 1.475 (1.470) | C1-N2-N3 | 112.51 (111.90) | C6-N2-C1-C5 | −172.15 (161.13) |
| N2-N3 | 1.369 (1.426) | C1-N2-C6 | 126.17 (108.00) | C9-C6-N2-C1 | −175.61 (−167.10) |
| N3-C4 | 1.294 (1.260) | C7-C4-N3 | 121.30 (120.00) | C7-C4-N3-N2 | −174.14178.90) |
| C4-C5 | 1.523 (1.497) | C8-C1-N2 | 113.59 (110.91) | C8-C1-N2-N3 | −103.74 (−137.88) |
| N2-C6 | 1.397 (1.462) | C9-C6-N2 | 120.81 (120.00) | C14-C8-C1-N2 | −151.46 (121.40) |
| C1-C8 | 1.525 (1.497) | C14-C8-C1 | 119.70 (120.00) | C19-C7-C4-N3 | −137.14 (−107.61) |
| C4-C7 | 1.475 (1.503) | C19-C7-C4 | 122.32 (120.00) | | |
| C20-C19 | 1.436 (1.497) | | | | |
| C11-C29 | 1.511 (1.719) | | | | |
| C16-F28 | 1.350 (1.320) | | | | |

*The values in the parenthesis are taken from reference [32]

C1 and C4 in the core ring respectively, are perpendicular to the same plane of given compounds. All small discrepancy that has been found for bond angles and dihedral angles computed for given compounds may be attributed to that the theoretical computations performed in the gas phase, but in the experimental ones conducted on the solid phase of a molecule.

## Vibrational Spectra Analysis

The experimental and computational IR spectra for compounds 13, 15,18 and 23 are given in Figs. 5, 6, 7, and 8.

The characteristic computed (unscaled and scaled) and experimental vibrational frequency values for compounds studied are presented in Tables 5, 6, 7, and 8.

As seen from figs and tables, the C-H stretching bands of aromatic rings for compounds computed are found in the range 3111–2926 $cm^{-1}$ and experimentally are observed at 3069–3032 $cm^{-1}$ in the functional group region of the spectrum in excellent agreement with simulated IR spectra. In the finger print region of the spectrum, both the C=C and the C=N stretching bands of aromatic rings for compounds computed are appeared in the range of 1545–1608 $cm^{-1}$ as compared with experimental that observed at 1493–1597 $cm^{-1}$ in good accordance for the simulated ones. The simulated deformations modes of the $CH_2$ and C-H for compounds are exhibited at 1436–1502 $cm^{-1}$ respectively and are observed experimentally at 1416–1502 $cm^{-1}$ in close corresponding agreement for vibrational frequencies. The C-F stretching bands of aromatic rings for compounds computed are found in the range 1234–1233 $cm^{-1}$ and experimentally are observed at 1219–1232 $cm^{-1}$ with great accordance for calculated frequencies. Furthermore, the rocking (ρ CH3) for compounds 15 and 23 are characterized at 968–1023 $cm^{-1}$ and are observed experimentally at 1000–980 $cm^{-1}$ respectively that are also agreed with computed frequency values. In addition to that, the C-Cl stretching bands of aromatic rings for compounds 13 and 18 are found at 527–540 $cm^{-1}$ and are observed experimentally at 559–525 $cm^{-1}$ respectively with a great agreement for their computed frequency values.

## UV-Vis Absorption and Fluorescence Emission Spectra Analysis

Time-dependent density function theory (TD-DFT) calculations were applied for computing the absorption and emission spectra at TD-DFT/B3LYP/6–31 G(d,p) level of theory for compounds 13,15,18 and 23.

The calculated absorption maxima ($\lambda_{max}$), excitation energies, oscillator strengths ($f$), and the calculated emission maxima($\lambda_{max}$) with a comparison of experimental data are given in Table 9.

The corresponding experimental, simulated UV-vis absorption and emission spectra are depicted in Fig. 9.

As seen from Fig. 9, selected compounds (13,15,18 and 23) experimentally exhibited two characteristic maximum absorption wavelengths ($\boldsymbol{\lambda_{max}}$) within 240 and 380 nm that were attributed to a π-π* and n-π* transitions, respectively. With comparison with the theoretical data presented in Fig. 10, we found a good agreement with absorption maxima for π-π* transitions with higher increasing for n-π* than the experimental ones. On the other hand, the theoretical emission maxima for four compounds (13,15,18 and 23) were found recorded much higher values shifts than the experimental ones as presented in Table 9 and Figs. 9 and 10, this may be attributed to the calculation of emission maxima in a vacuum in contrary for experimental ones that were measured in chloroform.

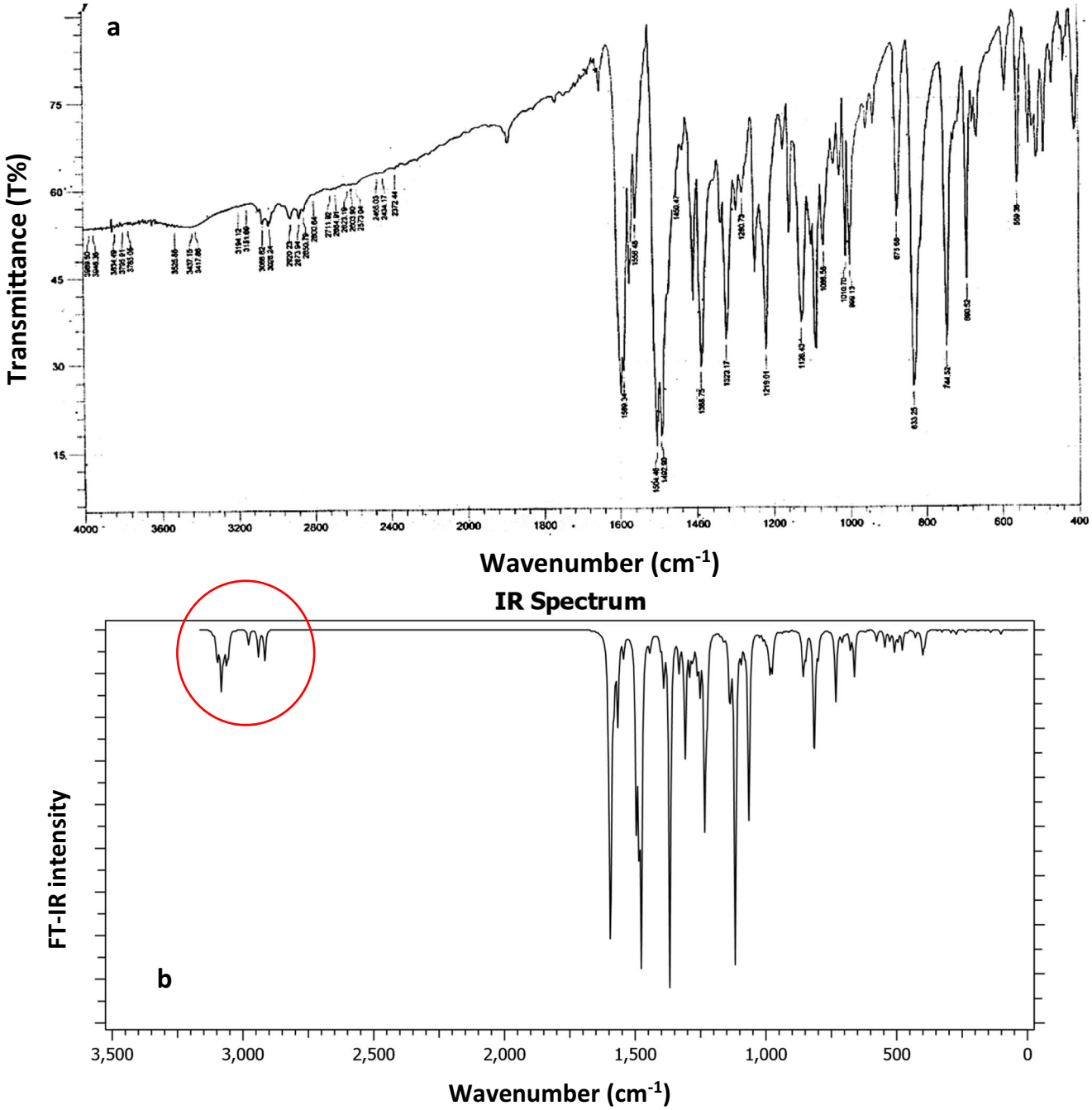


**Fig. 5** **a** Experimental and (**b**) Simulated IR spectra of compound 13 at DFT (B3LYP) with 6–31 G(d, p) basis set in gas phase

## Frontier Molecular Orbital Analysis

The two-pivotal molecular orbitals, one is highest occupied molecular orbital (HOMO) illustrates remotest molecular orbital filled by electron and acts as an electron donor. The other one is lowest unoccupied molecular orbital (LUMO) depicts inmost molecular orbital unfilled by electron and acts as an electron acceptor. These molecular orbitals are called the frontier molecular orbitals (FMOs). Between the highest occupied molecular orbital (HOMO) and lowest unoccupied molecular orbital (LUMO) creates energy gaps. This energy gap value provides a powerful tool to determine electronic transition, optical properties, kinetic stability and chemical reactivity of a molecule.

The dipole moment, optimized energy level, HOMO and LUMO energy values and energy gap values for compounds, 13, 15, 18 and 23 were computed via Gaussian 09 W program package at DFT/B3LYP method and 6-31G(d,p) basis set in the gas phase. The calculated data are given in Table 10.

As presented in Table 10, we found that the dipole moment of compound 18 is greater than all compounds and indicates

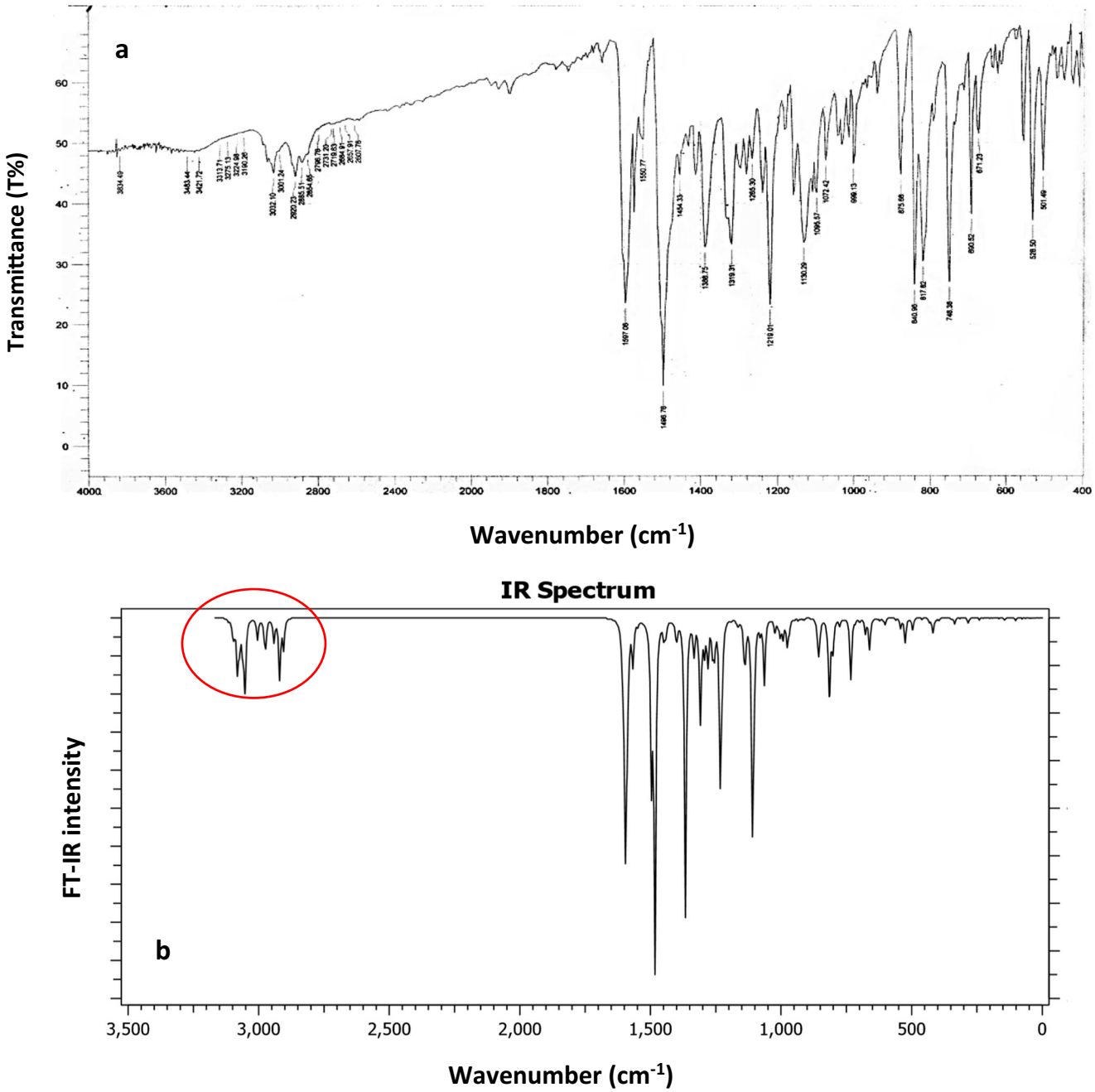


**Fig. 6** **a** Experimental and (**b**) Simulated IR spectra of compound 15 at DFT (B3LYP) with 6–31 G(d, p) basis set in gas phase

that it is more polar compound than the others. Also, energy gap value for compound 23 indicates that it is more reactive slightly than the others. In addition to that, all energy gap values ensure that all synthesized compounds are stable and polar compounds.

The 3D plots of frontier molecular orbitals of compounds 13,15,18 and 23 in gas phase are depicted in Fig. 11. As seen from Fig. 11 the HOMOs density of electrons for compounds, 13, 15, 18 and 23 are concentrated at the nitrogen atom of pyrazoline moiety with distribution over two rings at positions 1, and 3 at 2-pyrazoline moiety. The electronic transition of HOMO to LUMO was exhibited as charge transfer from the aromatic ring located at the position number one with respect to pyrazoline moiety with effective participation for the second aromatic ring in position number 3 at central pyrazoline moiety. On the other hand, the third aromatic ring attached at position five at central pyrazoline moiety appeared had no any participation in all electronic transition due to its spatial position out of the plane and it was remoted than central pyrazoline moiety. In overall these electronic transitions were attributed to a $\pi$ to $\pi^*$ transition.

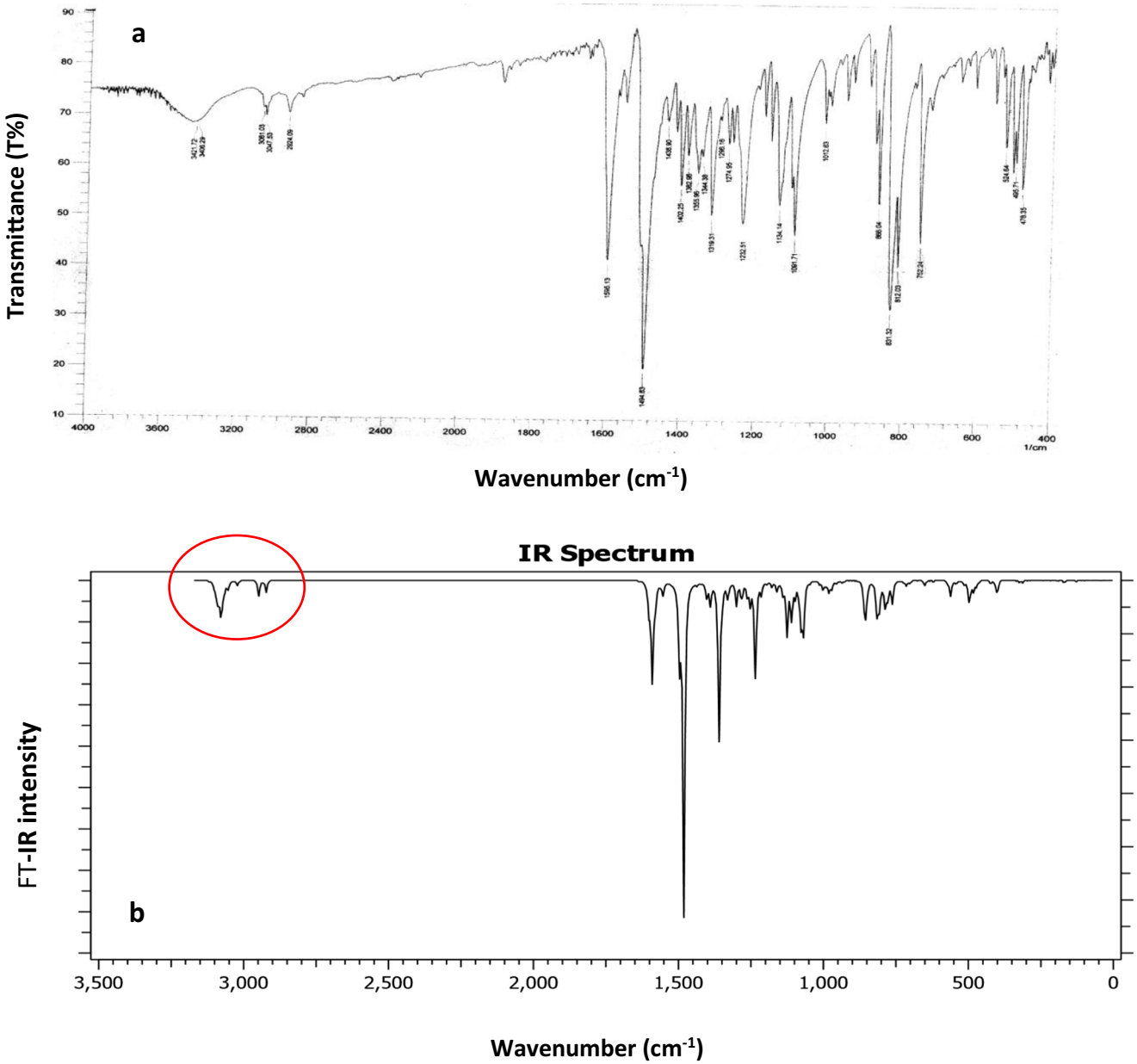


**Fig. 7** **a** Experimental and (**b**) Simulated IR spectra of compound 18 at DFT (B3LYP) with 6–31 G(d, p) basis set in gas phase

## Molecular Electrostatic Potential (MEP)

The molecular electrostatic potential (MEP) is a 3D plot implied charge distribution onto surfaces of molecules. It gives a profound prediction, interpretation for reactivity of both electrophilic and nucleophilic attack and hydrogen bonds interactions.

The molecular electrostatic potential for compounds 13,15,18 and 23 was computed via using the optimized molecular structures at the DFT/B3LYP method and 6-31G (d, p) basis set in the gas phase and visualized by Gaussian View 6.0 program package.

The 3D plots of the MEP for compounds 13,15,18 and 23 are given in Fig. 12.

As depicted in Fig. 12, the electrostatic potentials onto surfaces of compounds 13, 15,18 and 23 are exhibited with various colors. The color code map is in the range between (intense red) negative region to (intense blue) positive region. The electrostatic potentials decrease in the order blue> green> yellow>orange>red. Therefore, we can see from MEP map for compounds 13, 15, 18 and 23 the negative regions are basically localized onto both nitrogen atom labeled by (N3) presented at pyrazoline moiety and distributed over first aromatic ring attached by nitrogen atom labeled by (N2) at pyrazoline moiety with slightly distribution of negative electrostatic potentials onto the second aromatic ring attached by carbon atom labeled by (C4) at pyrazoline ring.

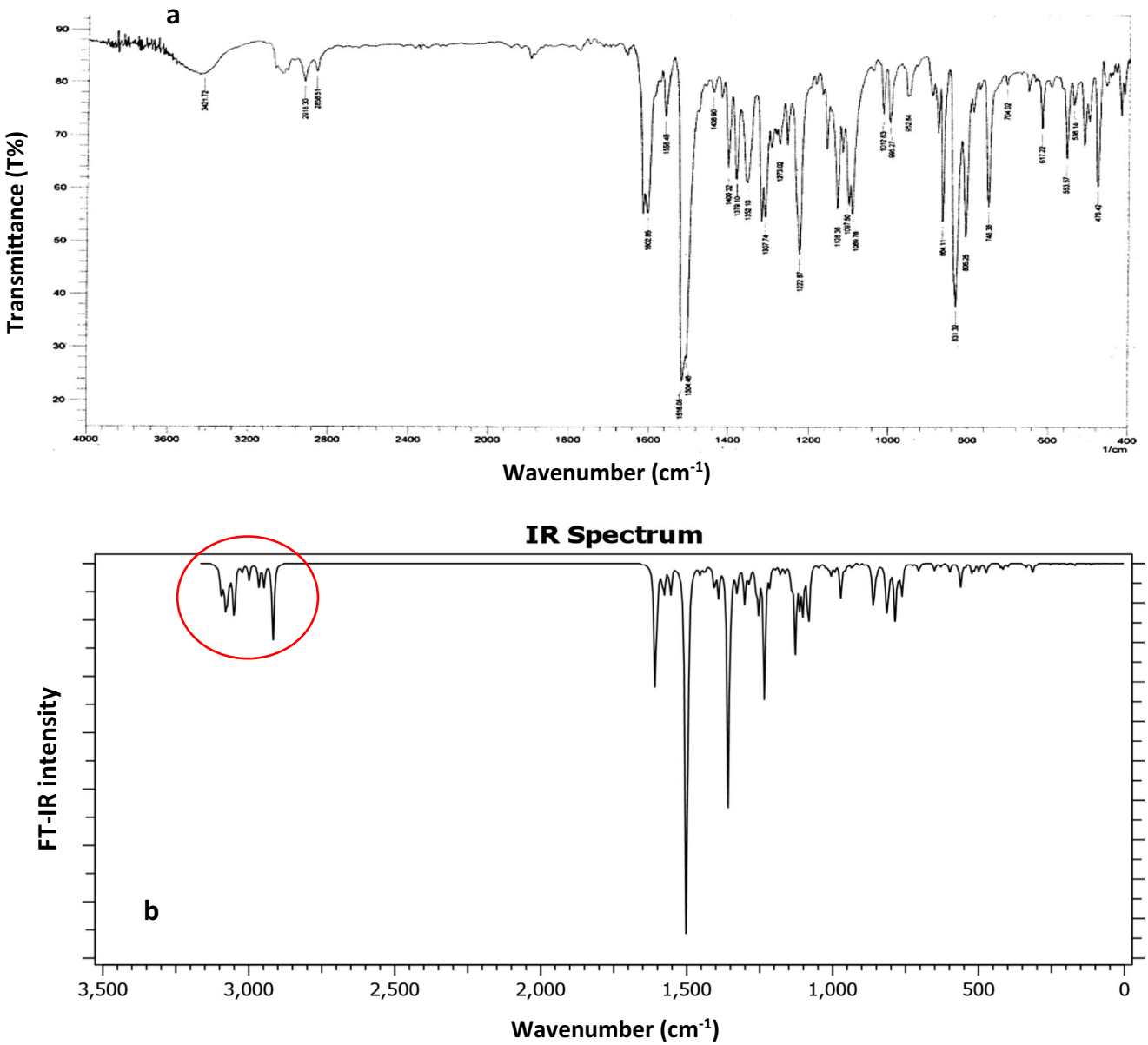


**Fig. 8** **a** Experimental and **b** Simulated IR spectra of compound 23 at DFT (B3LYP) with 6–31 G(d, p) basis set in gas phase

**Table 5** Experimental and calculated vibrational frequencies of compound 13

| Selected mode No. | Experimental vibration ($cm^{-1}$) | Theoretical vibration ($cm^{-1}$) | | Vibrational assignment |
|---|---|---|---|---|
| | | unscaled | scaled | |
| 1 | 3067 | 3241–3034 | 3116–2916 | ϒ C-H |
| 2 | 1589 | 1667 | 1603 | ϒ C=C (Ar, ring R) |
| 3 | 1558 | 1660 | 1596 | ϒ C=C (Ar, ring R") |
| 4 | 1504 | 1656 | 1592 | ϒ C=C (Ar, ring R') |
| 5 | 1493 | 1607 | 1545 | ϒ C=N |
| 6 | 1450 | 1536.20 | 1476.75 | β C-H |
| 7 | 1416 | 1497.93 | 1439.96 | β CH2 |
| 8 | 1389 | 1385.88 | 1332 | ϒ C-N |
| 9 | 1219 | 1284 | 1234 | ϒ C-F |
| 10 | 559 | 548 | 527 | ϒ C-Cl |

**Table 6** Experimental and calculated vibrational frequencies of compound 15

| Selected mode No. | Experimental vibration ($cm^{-1}$) | Theoretical vibration ($cm^{-1}$) | | Vibrational assignment |
|---|---|---|---|---|
| | | unscaled | scaled | |
| 1 | 3061.03 | 3242–3022 | 3117–2905 | ϒ C-H |
| 2 | 1597.06 | 1676 | 1608 | ϒ C=C (Ar, ring R) |
| 3 | 1551 | 1666 | 1602 | ϒ C=C (Ar, ring R') |
| 4 | 1497 | 1654.88 | 1596 | ϒ C=C (Ar, ring R") |
| 5 | 1489.05 | 1616 | 1549 | ϒ C=N |
| 6 | 1443.23 | 1540.71 | 1482.526473 | β C-H |
| 7 | 1418 | 1497.72 | 1439.75 | β CH2 |
| 8 | 1384.89 | 1352.34 | 1292.900435 | ϒ C-N |
| 9 | 1219.01 | 1284.49 | 1233.222931 | ϒ C-F |
| 10 | 1000 | 1006.99 | 968.019487 | ρ CH3 |

**Table 7** Experimental and calculated vibrational frequencies of compound 18

| Selected mode No. | Experimental vibration ($cm^{-1}$) | Theoretical vibration ($cm^{-1}$) | | Vibrational assignment |
|---|---|---|---|---|
| | | unscaled | scaled | |
| 1 | 3032.10 | 3243–3039 | 3118–2922 | ϒ C-H |
| 2 | 1595.13 | 1672.76 | 1608 | ϒ C=C (Ar, ring R) |
| 3 | 1562.03 | 1667.01 | 1602 | ϒ C=C (Ar, ring R") |
| 4 | 1494.83 | 1660 | 1596 | ϒ C=C (Ar, ring R') |
| 5 | 1438.90 | 1611 | 1549 | ϒ C=N |
| 6 | 1417 | 1560 | 1500 | β C-H |
| 7 | 1402.25 | 1495 | 1437 | β CH2 |
| 8 | 1382.96 | 1345 | 1292.900435 | ϒ C-N |
| 9 | 1232.51 | 1283 | 1233.222931 | ϒ C-F |
| 10 | 524.64 | 561 | 540 | ϒ C-Cl |

**Table 8** Experimental and calculated vibrational frequencies of compound 23

| Selected mode No. | Experimental vibration ($cm^{-1}$) | Theoretical vibration ($cm^{-1}$) | | Vibrational assignment |
|---|---|---|---|---|
| | | unscaled | scaled | |
| 1 | 3039 | 3236–3033 | 3111–2916 | ϒ C-H |
| 2 | – | 1675.84 | 1610.984992 | ϒ C=C (Ar, ring R) |
| 3 | 1602 | 1673.24 | 1608.485612 | ϒ C=C (Ar, ring R") |
| 4 | 1597.06 | 1666.16 | 1601.679608 | ϒ C=C (Ar, ring R') |
| 5 | 1558 | 1616.63 | 1554.066419 | ϒ C=N |
| 6 | 1504 | 1562.92 | 1502.434996 | β C-H |
| 7 | 1412 | 1493.93 | 1436 | β CH2 |
| 8 | 1381.03 | 1403.40 | 1349.08842 | ϒ C-N |
| 9 | 1220.94 | 1283.36 | 1233.693968 | ϒ C-F |
| 10 | 980 | 1064.01 | 1022.832813 | ρ CH3 |

**Table 9** The experimental, computed UV-Vis absorption and fluorescence emission spectra for compounds 13, 15, 18 and 23

| Compound | Experimental Absorption $\lambda_{max.}$ (nm) (in chloroform) | Theoretical Absorption $\lambda_{max.}$(nm) (Vacuum) | Excitation energy (ev) (Vacuum) | *f* (oscillator strength) (Vacuum) | Experimental emission $\lambda_{max.}$ (nm) (in chloroform) | Theoretical emission $\lambda_{max.}$(nm) (Vacuum) |
|---|---|---|---|---|---|---|
| 13 | 367 | 368.63 | 3.3634 | 0.6246 | 455.8 | 623.16 |
| 15 | 358 | 377.47 | 3.2846 | 0.2354 | 443.7 | 592.65 |
| 18 | 375 | 387.76 | 3.1974 | 0.3026 | 453.7 | 491.16 |
| 23 | 380 | 402.30 | 3.0819 | 0.2853 | 471.6 | 506.89 |

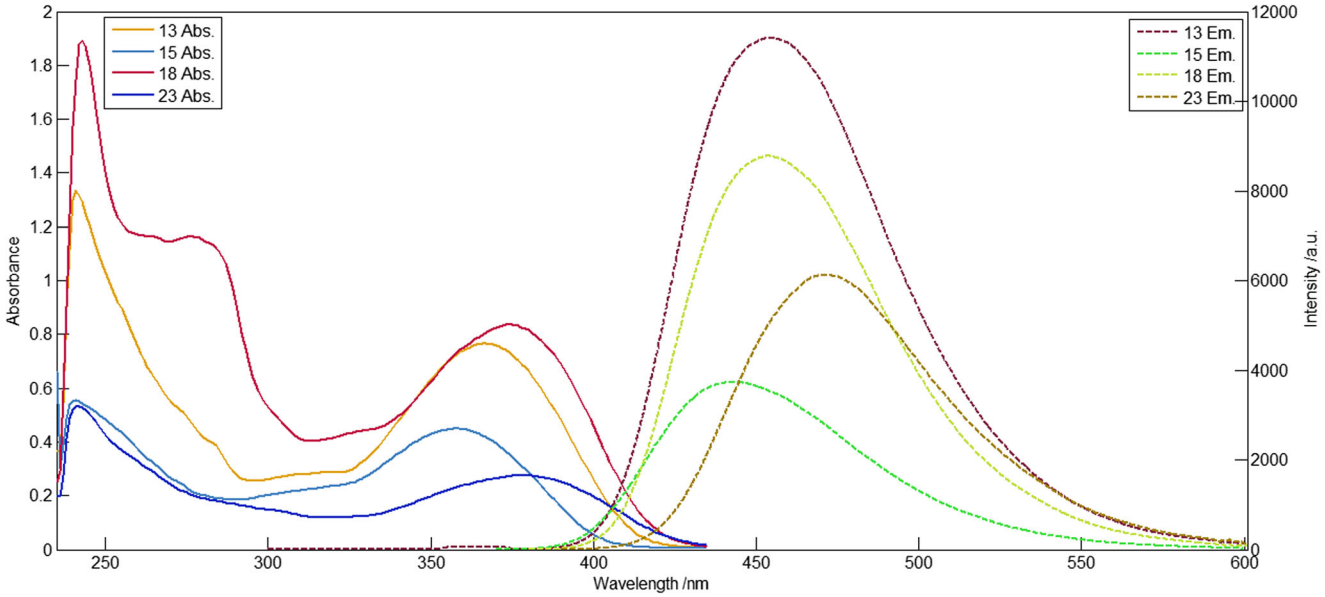


**Fig. 9** The experimental UV-Vis absorption and fluorescence emission spectra for compounds 13, 15, 18 and 23

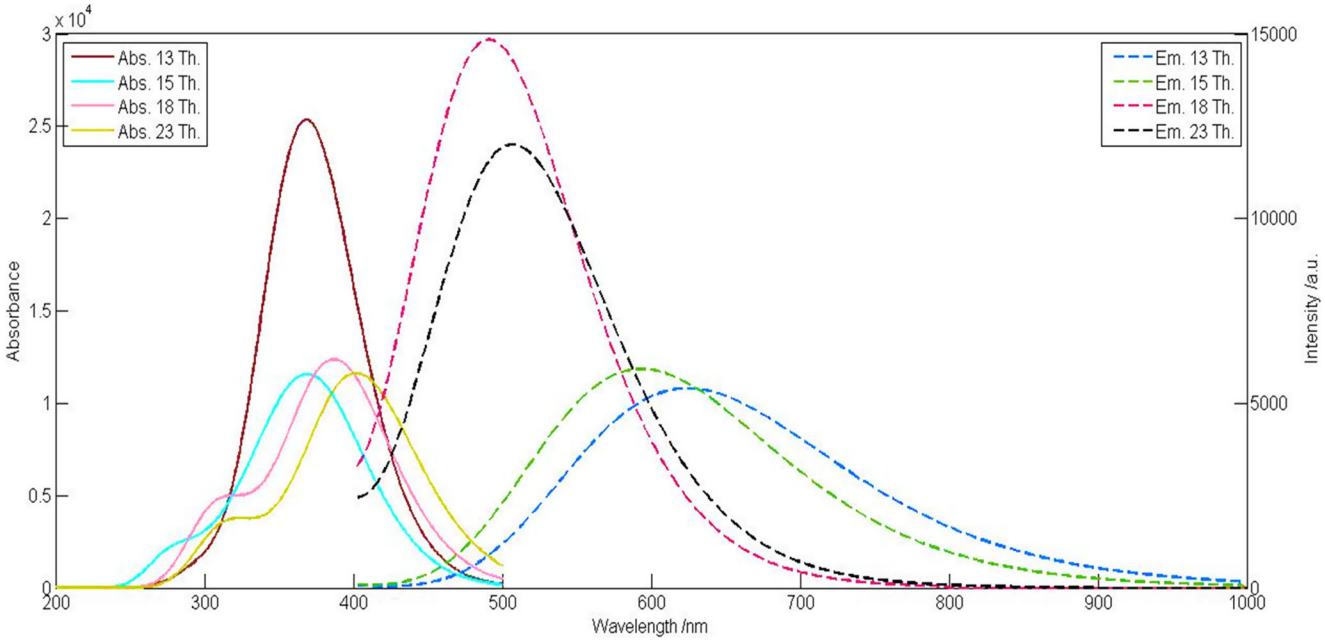


**Fig. 10** The simulated UV-Vis absorption and fluorescence emission spectra for compounds 13, 15, 18 and 23 computed at the DT-DFT/B3LYP/6-31G(d,p) level of theory in vacuum

**Table 10** The dipole moment, optimized energy level, HOMO LUMO energy values and energy gap values for compounds, 13, 15, 18 and 23

| Compounds | Dipole moment | Optimized energy level Kcal/mol | HOMO (a.u.) | LUMO (a.u.) | Energy gap values (eV) |
|---|---|---|---|---|---|
| 13 | 2.51 | 75.53 | −0.18658 | −0.05097 | 3.7 |
| 15 | 2.58 | 76.68 | −0.17985 | −0.03962 | 3.8 |
| 18 | 4.90 | 91.02 | −0.18766 | −0.05373 | 3.6 |
| 23 | 2.25 | 92.17 | −0.17827 | −0.04887 | 3.5 |

On the other hand, the positive regions hovered onto the third aromatic ring attached by carbon atom labeled by (C1) at pyrazoline ring for compounds 13,15,18 and 23. Addition to that the zero potential regions also were appeared in green color for all compounds studies.

## NMR Spectra Analysis

The optimized molecular structures of the active novel pyrazoline compounds 13, 15,18, and 23 are used to compute the NMR spectra using the DFT at B3LYP method via 6–311 + G(2d,p) basis set in the gas phase through the GIAO method. The theoretical $^{1}H$ and $^{13}C$ NMR chemical shifts values for compounds 13, 15,18 and 23 were computed at the same level of the theory in ppm relative to TMS. The calculated $^{1}H$ and $^{13}C$ NMR chemical shifts values for compounds 13, 15,18 and 23 are given in Tables 11, 12, 13, and 14.

As appeared in Table 11, for compound 13, the experimental and calculated carbon-13 chemical shifts values for C5 and C1 atoms were found to be 43.4/46.6 ppm (exp./cal.) and 64.0/68.55 ppm (exp./cal.) respectively which are attributed to the presence of pyrazolinyl carbon atoms. Furthermore, the experimental and calculated

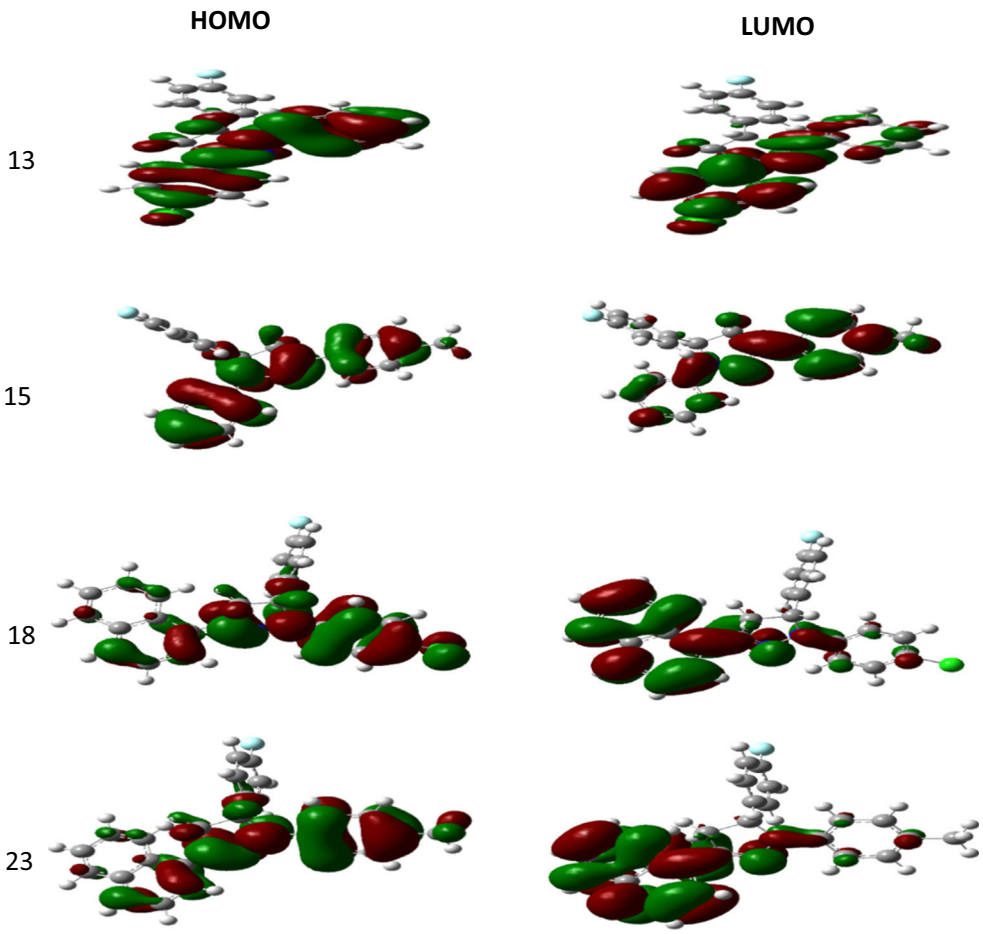


**Fig. 11** The 3D plots of frontier molecular orbitals for compounds 13,15,18 and 23 in gas phase with their energy levels computed at the DFT/B3LYP/6-31G (d,p) level of theory

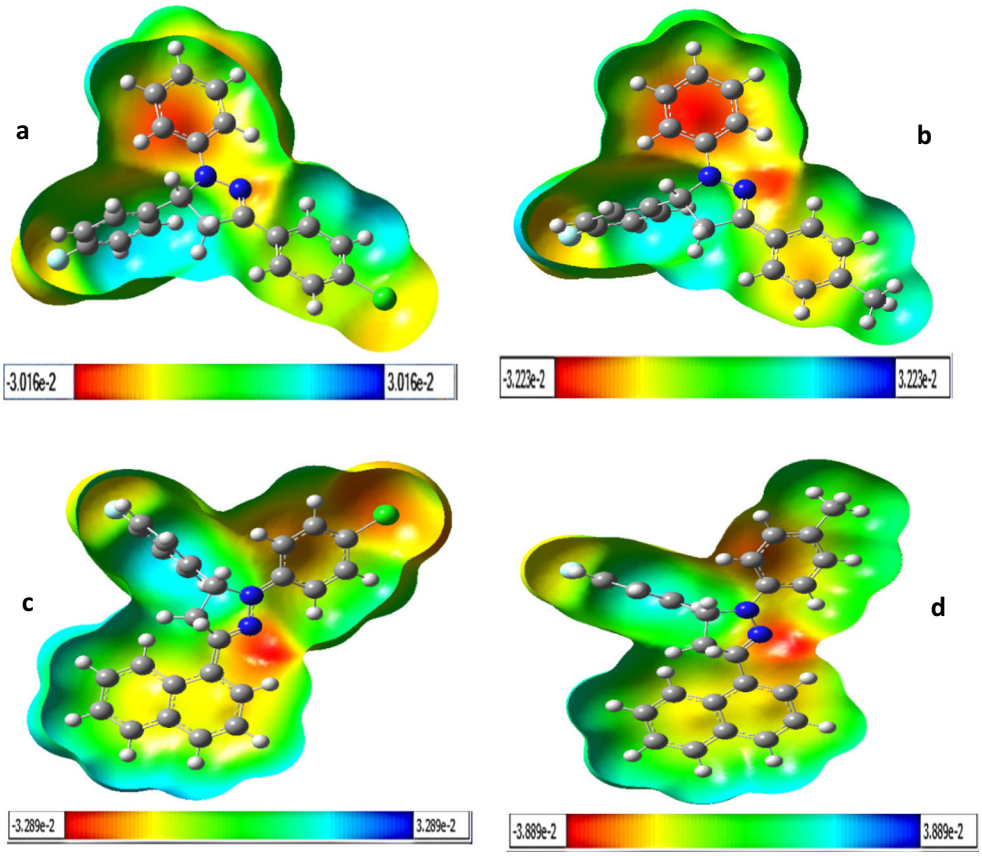


**Fig. 12** The 3D plots of MEP surfaces for (**a**) compound 13, (**b**) compound 15, (**c**) compound 18, and (**d**) compound 23 computed at the DFT/B3LYP/6-31G(d,p) level of theory (a.u.)

**Table 11** The experimental and computed $^{1}H$ and $^{13}C$ NMR isotropic chemical shifts values in ppm (with respect to TMS) for compound 13

| Atom position | Exp. Chemical shifts (ppm) (in $CHCl_3$-d) | Cal. Chemical shifts (ppm) (in gas) | Atom position | Exp. Chemical shifts (ppm) (in $CHCl_3$-d) | Cal. Chemical shifts (ppm) (in gas) |
|---|---|---|---|---|---|
| H26 | 5.28 | 5.2068 | C1 | 64.0 | 68.5503 |
| H27 | 3.81 | 3.7751 | C4 | 161.0 | 147.802 |
| H28 | 3.08 | 2.8809 | C5 | 43.4 | 46.6295 |
| H29 | 6.78–6.85 | 6.3482 | C6 | 145.6 | 149.1618 |
| H30 | 7.01–7.43 | 7.14665 | C7 | 138.0 | 137.1413 |
| H31 | 7.01–7.43 | 6.9485 | C8 | 138.1 | 145.9706 |
| H32 | 7.43 | 7.5235 | C9 | 113.5 | 113.9104 |
| H33 | 7.85 | 8.0703 | C10 | 131.2 | 132.5427 |
| H34 | 6.85 | 7.0479 | C11 | 125.5 | 122.8455 |
| H35 | 7.43 | 7.3731 | C12 | 127.6 | 133.7771 |
| H36 | 7.67 | 7.6432 | C13 | 119.5 | 118.0874 |
| H37 | 7.86 | 8.6209 | C14 | 129.5 | 129.5009 |
| H38 | 7.01–7.43 | 7.5235 | C15 | 127.1 | 132.3916 |
| H39 | 7.01–7.43 | 7.2576 | C16 | 128.9 | 147.4773 |
| H40 | 7.18 | 7.14665 | C17 | 134.4 | 133.477 |
| H41 | 7.43 | 7.5235 | C18 | 129.0 | 130.5276 |
| | | | C19 | 131.2 | 131.3034 |
| | | | C20 | 116.2 | 119.36 |
| | | | C21 | 163.4 | 171.4658 |
| | | | C22 | 119.5 | 120.6984 |
| | | | C23 | 129.1 | 131.7185 |

**Table 12** The experimental and computed $^{1}H$ and $^{13}C$ NMR isotropic chemical shifts values in ppm (with respect to TMS) for compound 15

| Atom position | Exp. Chemical shifts (ppm) (in $CHCl_3$-d) | Cal. Chemical shifts (ppm) (in gas) | Atom position | Exp. Chemical shifts (ppm) (in $CHCl_3$-d) | Cal. Chemical shifts (ppm) (in gas) |
|---|---|---|---|---|---|
| H26 | 5.24 | 5.2349 | C1 | 63.8 | 69.129 |
| H27 | 3.82 | 3.8671 | C4 | 160.9 | 150.6207 |
| H28 | 3.10 | 2.9616 | C5 | 43.7 | 47.5153 |
| H29 | 7.189 | 7.181966667 | C6 | 145.0 | 150.4999 |
| H30 | 7.298 | 7.29165 | C7 | 144.9 | 147.9064 |
| H31 | 7.327 | 7.60615 | C8 | 138.5 | 137.4028 |
| H32 | 7.642 | 8.7183 | C9 | 119.2 | 129.4482 |
| H33 | 6.792 | 6.4208 | C10 | 127.6 | 132.5141 |
| H34 | 7.166 | 7.181966667 | C11 | 138.8 | 145.922 |
| H35 | 7.025 | 6.9795 | C12 | 138.4 | 134.005 |
| H36 | 7.309 | 7.60615 | C13 | 125.87 | 130.5536 |
| H37 | 7.614 | 8.1416 | C14 | 113.4 | 114.5931 |
| H38 | 7.281 | 7.60615 | C15 | 129.0 | 133.39915 |
| H39 | 7.222 | 7.29165 | C16 | 125.76 | 123.1601 |
| H40 | 7.074 | 7.181966667 | C17 | 129.9 | 134.5399 |
| H41 | 7.374 | 7.60615 | C18 | 116.1 | 118.9418 |
| H42 | 2.04 | 2.0112 | C19 | 127.5 | 132.1449 |
| H43 | 2.39 | 2.55655 | C20 | 115.9 | 120.2121 |
| H44 | 2.39 | 2.55655 | C21 | 163.4 | 172.3871 |
| | | | C22 | 125.45 | 121.7053 |
| | | | C23 | 129.31 | 133.39915 |
| | | | C25 | 21.42 | 22.4881 |

carbon-13 chemical shifts values for aromatic rings have been exhibited at the interval 113.5–163.4/113.91–171.47 ppm (exp./cal.). On the other hand, the experimental and calculated $^{1}H$ NMR chemical shifts values for H28, H27, and H26 atoms appeared at 3.08/2.88 ppm (exp./cal.), 3.81/3.78 ppm and 5.28/5.21 ppm (exp./cal.) respectively which are attributed to the upfield of the methylene protons, downfield of methylene protons and methine proton respectively. In the same circumstance, the experimental and calculated $^{1}H$ NMR chemical shifts values for aromatic rings have been exhibited at the interval 6.78–7.65/6.35–8.62 ppm (exp./cal.).

Similarly, in Table 12 for compound 15, the experimental and calculated carbon-13 chemical shifts values for C29, C5 and C1 atoms were found to be 21.42/22.49 ppm (exp./cal.), 43.7/47.52 ppm (exp./cal.) and 63.8/69.13 ppm (exp./cal.) respectively which are attributed to presence of 4-methylphenyl, pyrazolinyl carbon atoms respectively. Furthermore, the experimental and calculated carbon-13 chemical shifts values for aromatic rings have been exhibited at the interval 113.4–163.4/114.59–172.39 ppm (exp./cal.). On the other hand, the experimental and calculated $^{1}H$ NMR chemical shifts values for H42, H43, H44, H28, H27, and H26 atoms appeared at 2.04/2.01 ppm (exp./cal.), 2.39/2.56 ppm (exp./cal.), 2.39/2.56 ppm (exp./cal.), 3.10/2.96 ppm (exp./cal.), 3.82/3.87 ppm (exp./cal.) and 5.24/5.23 ppm (exp./cal.) respectively which are attributed to 4-methylphenyl, upfield of the methylene protons, downfield of methylene protons and methine proton respectively. In the same circumstance, the experimental and calculated $^{1}H$ NMR chemical shifts values for aromatic rings have been exhibited at the interval 6.79–7.64/6.42–8.72 ppm (exp./cal.).

As given in Table 13 for compound 18, the experimental and calculated carbon-13 chemical shifts values for C5 and C1 atoms were found to be at 43.6/51.15 ppm (exp./cal.) and 63.9/68.17 ppm (exp./cal.) respectively which are attributed to presence of pyrazolinyl carbon atoms. Furthermore, the experimental and calculated carbon-13 chemical shifts values for aromatic rings have been exhibited at the interval 114.6–163.5/115.09–172.56 ppm (exp./cal.). On the other hand, the experimental and calculated 1H NMR chemical shifts values for H31, H32 and H30 atoms were appeared at 3.25/3.64 ppm (exp./cal.), 3.93/3.80 ppm (exp./cal.) and 5.26/5.46 ppm (exp./cal.) respectively which are attributed to the upfield of the methylene protons, downfield of methylene protons and methine proton respectively. In the same

**Table 13** The experimental and computed $^{1}H$ and $^{13}C$ NMR isotropic chemical shifts values in ppm (with respect to TMS) for compound 18

| Atom position | Exp. Chemical shifts (ppm) (in $CHCl_3$-d) | Cal. Chemical shifts (ppm) (in gas) | Atom position | Exp. Chemical shifts (ppm) (in $CHCl_3$-d) | Cal. Chemical shifts (ppm) (in gas) |
|---|---|---|---|---|---|
| H30 | 5.26 | 5.4604 | C1 | 63.9 | 68.1653 |
| H31 | 3.25 | 3.6356 | C4 | 161.0 | 154.6006 |
| H32 | 3.93 | 3.7981 | C5 | 43.6 | 51.146 |
| H33 | 7.50–7.53 | 7.581 | C6 | 137.7 | 138.8301 |
| H34 | 7.50–7.53 | 7.4142 | C7 | 147.4 | 147.5239 |
| H35 | 7.28–7.32 | 7.2387 | C8 | 143.1 | 144.8397 |
| H36 | 7.50–7.53 | 7.581 | C9 | 127.9 | 132.6902 |
| H37 | 8.17 | 8.14955 | C10 | 116.1 | 121.0626 |
| H38 | 7.50–7.53 | 7.581 | C11 | 163.5 | 172.5648 |
| H39 | 7.16–7.19 | 7.1671 | C12 | 123.4 | 121.4739 |
| H40 | 7.03–7.08 | 6.3462 | C13 | 128.3 | 133.0346 |
| H41 | 8.17 | 8.14955 | C14 | 116.3 | 119.3409 |
| H42 | 7.81–7.88 | 7.8379 | C15 | 130.0 | 135.4526 |
| H43 | 8.17 | 8.14955 | C16 | 133.6 | 138.3028 |
| H44 | 7.81–7.88 | 7.9747 | C17 | 128.9 | 133.6708 |
| H45 | 7.81–7.88 | 7.6469 | C18 | 114.6 | 115.0892 |
| H46 | 7.81–7.88 | 7.7687 | C19 | 133.3 | 138.1509 |
| H47 | 8.17 | 8.14955 | C20 | 137.8 | 140.2124 |
| | | | C21 | 129.2 | 134.6453 |
| | | | C22 | 126.59 | 129.8035 |
| | | | C23 | 128.1 | 133.1754 |
| | | | C24 | 126.58 | 129.4909 |
| | | | C25 | 127.6 | 130.4613 |
| | | | C26 | 127.5 | 130.2224 |
| | | | C27 | 130.0 | 134.4285 |

circumstance the experimental and calculated $^{1}H$ NMR chemical shifts values for aromatic rings have been exhibited at the interval 7.50–8.17/6.35–8.15 ppm (exp./cal.). lastly, as presented in Table 14 for compound 23, the experimental and calculated carbon-13 chemical shifts values for C25, C5 and C1 atoms were found to be 20.5/19.78 ppm (exp./cal.), 43.5/52.56 ppm (exp./cal.) and 64.2/73.59 ppm (exp./cal.) respectively which are attributed to presence of 4-methylphenyl, pyrazolinyl carbon atoms respectively. Furthermore, the experimental and calculated carbon-13 chemical shifts values for aromatic rings have been exhibited at the interval 113.6–163.4/119.86–172.68 ppm (exp./cal.). On the other hand, the experimental and calculated $^{1}H$ NMR chemical shifts values for H50, H49, H48, H31and H30 atoms appeared at 2.28/1.85 ppm (exp./cal.), 2.28/1.35 ppm (exp./cal.), 2.28/1.45 ppm (exp./cal.), 3.25/3.47 ppm (exp./cal.), and 5.27–5.32/4.94 ppm (exp./cal.) respectively which are attributed to 4-methylphenyl, upfield of the methylene protons, downfield of methylene protons and methine proton respectively. In the same circumstance, the experimental and calculated $^{1}H$ NMR chemical shifts values for aromatic rings have been exhibited at the interval 7.01–8.19/6.15–13.98 ppm (exp./cal.).

In general, all the theoretical $^{1}H$ and $^{13}C$ NMR chemical shifts values for compounds 13, 15,18 and 23 have been observed in accordance with experimental data that were seen in Tables 11, 12, 13 and 14 with slight deviation in some values experimentally due to the computational simulation of calculations were performed in the gas phase. The corresponding figures for experimental and theoretical charts of $^{1}H$ and $^{13}C$ NMR chemical shifts values for compounds 13, 15,18 and 23 were given in Figs. (1S–8S).

## Conclusion

In the present work, four active new synthesized compounds were selected from twenty-one analogues due to their high fluorescence quantum yield values than the reference value (quinine sulfate) and were characterized chemically and spectrally. Density functional theory (DFT) computations, FT-IR, UV-visible, emission spectra

**Table 14** The experimental and computed $^{1}H$ and $^{13}C$ NMR isotropic chemical shifts values in ppm (with respect to TMS) for compound 23

| Atom position | Exp. Chemical shifts (ppm) (in $CHCl_3$-d) | Cal. Chemical shifts (ppm) (in gas) | Atom position | Exp. Chemical shifts (ppm) (in $CHCl_3$-d) | Cal. Chemical shifts (ppm) (in gas) |
|---|---|---|---|---|---|
| H30 | 5.27–5.32 | 4.9383 | C1 | 64.2 | 73.5923 |
| H31 | 3.25 | 3.4711 | C4 | 160.9 | 169.8879 |
| H32 | 7.28–7.36 | 7.24956 | C5 | 43.5 | 52.5579 |
| H33 | 8.19 | 8.0538 | C6 | 151.60 | 160.3263 |
| H34 | 7.28–7.36 | 7.24956 | C7 | 137.87 | 137.3657 |
| H35 | 7.04–7.08 | 6.6816 | C8 | 143.65 | 143.9017 |
| H36 | 7.04–7.08 | 6.55445 | C9 | 126.03 | 126.0289 |
| H37 | 7.28–7.36 | 7.24956 | C10 | 137.20 | 133.2094 |
| H38 | 7.04–7.08 | 6.55445 | C11 | 142.53 | 140.8829 |
| H39 | 7.04–7.08 | 6.151 | C12 | 130.64 | 131.2733 |
| H40 | 8.19 | 8.0538 | C13 | 124.14 | 124.3045 |
| H41 | 7.81–7.88 | 7.8652 | C14 | 133.61 | 132.5076 |
| H42 | 7.81–7.88 | 7.4811 | C15 | 116.14 | 120.2861 |
| H43 | 7.81–7.88 | 8.5717 | C16 | 163.4 | 172.6833 |
| H44 | 7.81–7.88 | 13.9847 | C17 | 123.46 | 119.8602 |
| H45 | 7.28–7.36 | 7.24956 | C18 | 146.37 | 149.288 |
| H46 | 7.28–7.36 | 7.24956 | C19 | 130.06 | 130.631 |
| H47 | 7.48–7.51 | 7.7481 | C20 | 133.41 | 131.8662 |
| H48 | 2.28 | 1.4488 | C21 | 133.33 | 131.4031 |
| H49 | 2.28 | 1.3519 | C22 | 127.83 | 127.8162 |
| H50 | 2.28 | 1.8524 | C23 | 127.78 | 127.2452 |
| | | | C24 | 129.52 | 129.7057 |
| | | | C25 | 126.27 | 126.0798 |
| | | | C26 | 127.59 | 127.1244 |
| | | | C27 | 129.69 | 129.7807 |
| | | | C29 | 20.5 | 19.771 |

and NMR spectra for the optimized molecular structures were successfully performed in good agreement with experimental data. Via the HOMO-LUMO analysis and MEP maps, we could track and determine electron density onto the surfaces, chemical stability, reactivity and dipole moment for selected compounds. The computational studies could be a powerful tool that could assist experimental data for illustration and prediction optical properties for given compounds in an excellent visualization.

**Acknowledgements** Authors thank anyone who helped us to publish these valuable data presented in our manuscript.

**Authors' Contributions** The authors worked jointly on every section of the paper. Both authors read and approved the final manuscript.

**Funding** Authors carried all experiments on their expenses without support from any organization.

## Compliance with Ethical Standards

**Ethics Approval and Consent to Participate** Not applicable.

**Consent for Publication** Our manuscript didn't contain any individual person's data in any form.

**Competing Interests** The authors declare that they have no competing interests.

## References

1. Lone I, Khan K, Fozdar B (2014) Synthesis, physicochemical properties, antimicrobial and antioxidant studies of pyrazoline derivatives bearing a pyridyl moiety. Med Chem Res 23:363–369
2. Lv P-C, Li D-D, Li Q-S, Lu X, Xiao Z-P, Zhu H-L (2011) Synthesis, molecular docking and evaluation of thiazolylpyrazoline derivatives as EGFR TK inhibitors and potential anticancer agents. Bioorg Med Chem Lett 21:5374–5377
3. Babu VH, Sridevi C, Joseph A, Srinivasan KK (2008) Synthesis and biological evaluation of some novel pyrazolines. Indian J Pharm Sci 69:470–473
4. West RC (ed) (1974) CRC Handbook of Chemistry and Physics, 5th edn. CRC Press, Cleveland
5. Li JF, Guan B, Li DX, Dong C (2007) Study on the fluorescence properties of a new intramolecular charge transfer compound 1,5-

diphenyl-3-(N-ethylcarbazole-3-yl)-2-pyrazoline. Spectrochim Acta A 68:404–408
6. Hasan A, Abbas A, Akhtar MN (2011) Synthesis, characterization and fluorescent property evaluation of 1, 3, 5-triaryl-2-pyrazolines. Molecules 16:7789–7802
7. Zimmer H, Armbruster DC, Trauth LJ (1965) The aldol condensation of aromatic aldehydes with N-Acetyl-2-pyrrolidinone: synthesis of 3-Arylidene-2-pyrrolidinones. J Heterocyclic Chem 2:171
8. Hedaya E, Theodoropulos S (1968) The preparation and reactions of stable phosphorus ylides derived from maleic anhydrides, maleimides or isomaleimides. Tetrahedron 24:2241
9. Ichikawa M, Masuhara H, Maus M, Rettig W (1996) Radiative depopulation of the excited intramolecular charge-transfer state of 9-(4-(*N*,*N*-Dimethylamino)phenyl)phenanthrene. J Am Chem Soc 118:2892
10. Abbas A, Hussain S, Hafeez N, Naseer MM (2014) Synthesis and spectral characterization of new homologous 1,3,5-triaryl-2-pyrazolines: influence of alkyloxy chain length on fluorescence. Spectrochim Acta A 133:182–189
11. Lu B, Zhang J, Wang M, Zhou Y, Chen X (2012) Synthesis and fluorescent property of pyrazoline derivatives. Chin J Chem 30: 1345–1350
12. Ozdemir A, Turan-Zitouni G, Kaplancikli ZA et al (2007) Synthesis and antimicrobial activity of 1-(4-aryl-2-thiazolyl)-3-(2-thienyl)-5-aryl-2-pyrazoline derivatives. Eur J Med Chem 42:403–409
13. Bian B, Ji S-J, Shi H-B (2008) Synthesis and fluorescent property of some novel bischromophore compounds containing pyrazoline and naphthalimide groups. Dyes Pigments 76:348–352
14. Babar A, Khalid H, Ayub K, Saleem S, Waseem A, Mahmood T, Munawar MA, Abbas G, Khan AF (2014) Synthesis, characterization and density functional theory study of some new 2-anilinothiazoles. J Mol Struct 1072:221–227
15. Kapturkiewicz A, Herbich J, Karpiuk J, Nowacki J (1997) Intramolecular radiative and radiationless charge recombination processes in donor−acceptor carbazole derivatives. J Phys Chem A 101:2332
16. Braun D, Retting W, Delmond S, Letard JF, Lapouyade R (1997) Amide derivatives of DMABN: a new class of dual fluorescent compounds. J Phys Chem A 101:6836
17. Wang P, Wu S (1995) Spectroscopy and photophysics of bridged enone derivatives: effect of molecular structure and solvent. J Photochem Photobiol A Chem 86:109
18. Wang SL, Ho TI (2000) Substituent effects on intramolecular charge-transfer behaviour of styrylheterocycles. J Photochem Photobiol A Chem 135:119
19. Hashimoto M, Hamaguchi H (1995) Molecular layer-by-layer engineering of superconducting and superionic materials in the $(AgI)Bi_2Sr_2CaCu_2O_y$ system. J Phys Chem 99:7875
20. Grabowski ZR (1993) Electron transfer in flexible molecules and molecular ions. Pure Appl Chem 65:1751
21. Yan ZL, Hu GW, Wu SK (1995) A study on the photophysical 8ehaviors of 1, 5—Diphenyl-3-naphthyl-2-pyrazoline compound. Acta Chim Sin 53:227
22. Wagner A, Schellhammer CW, Petersen S (1966) Aryl-$\Delta^2$-pyrazolines as optical brighteners. Angew Chem Int Ed Eng 5:699
23. Wang P, Komatsuzaki NO, Himeda Y, Sugihara H, Arakawa H, Kasuga K (2001) 3-(2-Pyridyl)-2-pyrazoline derivatives: novel fluorescent probes for $Zn^{2+}$ion. Tetrahedron Lett 42:9199
24. Girgis AS, Basta AH, El-Saied H, Mohamed MA, Bedair AH, Salim AS (2018) Synthesis, quantitative structure–property relationship study of novel fluorescence active 2-pyrazolines and application. R Soc Open Sci 5:171964
25. Frisch MJ, Trucks GW, Schlegel HB, Scuseria GE, Robb MA, Cheeseman JR, Scalmani G, Barone V, Mennucci B, Petersson GA, Nakatsuji H, Caricato M, Li X, Hratchian HP, Izmaylov AF, Bloino J, Zheng G, Sonnenberg JL, Hada M, Ehara M, Toyota K, Fukuda R, Hasegawa J, Ishida M, Nakajima T, Honda Y, Kitao O, Nakai H, Vreven T, Montgomery Jr JA, Peralta JE, Ogliaro F, Bearpark M, Heyd JJ, Brothers E, Kudin KN, Staroverov VN, Kobayashi R, Normand J, Raghavachari K, Rendell A, Burant JC, Iyengar SS, Tomasi J, Cossi M, Rega N, Millam JM, Klene M, Knox JE, Cross JB, Bakken V, Adamo C, Jaramillo J, Gomperts R, Stratmann RE, Yazyev O, Austin AJ, Cammi R, Pomelli C, Ochterski JW, Martin RL, Morokuma K, Zakrzewski VG, Voth GA, Salvador P, Dannenberg JJ, Dapprich S, Daniels AD, Farkas O, Foresman JB, Ortiz JV, Cioslowski J, Fox DJ (2009) Gaussian, Inc, Wallingford CT
26. Dennington R, Keith TA, Millam JM (2016) GaussView, Version 6, Semichem Inc., Shawnee Mission, KS
27. Becke AD (1993) Density-functional thermochemistry. III. The role of exact exchange. J ChemPhys 98:5648–5652
28. Lee C, Yang W, Parr RG (1988) Development of the Colle-Salvetti correlation-energy formula into a functional of the electron density. Physiol Res B37:785–789
29. Chinnaraja D, Rajalakshmi R, Srinivasan T, VelmuruganbJ D (2014) Jayabharathi, Spectral studies of 2-pyrazoline derivatives: Structural elucidation through single crystal XRD and DFT calculations. Spectrochim Acta A 124:30–33
30. Ibrahim MM, Al-Refai M, Ayub K, Ali BF (2016) Synthesis, Spectral Characterization and Fluorescent Assessment of 1,3,5-Triaryl-2-pyrazoline Derivatives: Experimental and Theoretical Studies. J Fluoresc 26:1447–1455
31. Agrawal M, Sonar PK, Saraf SK (2011) Synthesis of 1,3,5-trisubstituted pyrazoline nucleus containing compounds and screening for antimicrobial activity. Med Chem Res 21:3376–3381
32. Bhandari S, Tripathi AC, Saraf SK (2013) Novel 2-pyrazoline derivatives as potential anticonvulsant agents. Med Chem Res 22: 5290–5296